

Spatio-temporal variation in rainfall-runoff erosivity due to climate change in the Lower Niger Basin, West Africa

Amobichukwu C. Amanambu^{a,b,f}, Lanhai Li^{a,b,c,*}, Christiana N. Egbinola^e, Omon A. Obarein^d, Christophe Mupenzi^{a,b,g}, Ditao Chen^{a,b}

^a State Key Laboratory of Desert and Oasis Ecology, Xinjiang Institute of Ecology and Geography, Chinese Academy of Sciences, 818 South Beijing Road, Urumqi 830011, Xinjiang, China

^b University of Chinese Academy of Sciences, Beijing 100049, China

^c Yili Station for Watershed Ecosystem Studies, 818 South Beijing Road, Urumqi 830011, Xinjiang, China

^d Department of Geography, Kent State University, 325 S Lincoln St., Kent, OH 44242, USA

^e Department of Geography, University of Ibadan, Ibadan, Oyo State, Nigeria.

^f Water, Engineering, and Development Center, School of Civil and Building Engineering, Loughborough University, Leicestershire, UK

^g University of Lay Adventists of Kigali (UNILAK), P.O. Box 6392, Kigali, Rwanda

ARTICLE INFO

Keywords:

Rainfall-runoff erosivity
GCMs
RUSLE
Soil erosion
Niger-basin
Climate change

ABSTRACT

Spatio-temporal variation in rainfall-runoff erosivity resulting from changes in rainfall characteristics due to climate change has implications for soil and water conservation in developing countries. Understanding past and future variations in rainfall-runoff erosivity and its implication, in tropical areas where there are limited continuous daily rainfall records, is important. The present study attempted to (i) quantify the nature of spatio-temporal variability of erosivity from rainfall amount using Global Circulation Models (GCMs), and (ii) evaluate the implications of changes in rainfall-runoff erosivity in the Lower Niger Basin, West Africa. The GCMs scenarios (GFDLCM3, HADCM2, MIROC5, and MPIESMLR) were statistically downscaled using the delta method for three-time slices (the 2030s, 2050s, and 2070s). World climate data was used as the current baseline climate since it is the source of the future precipitation simulation. The R factor from the Revised Soil Loss Equation (RUSLE) was used to determine erosivity, while the RUSLE model was used to ascertain the implications of changes in erosivity. Observation data (1970–2013) from 20 meteorological stations were used to validate the erosivity model. The result indicates that there is an increasing trend in the annual rainfall-runoff erosivity from the baseline climate up to the GCMs, for all the GCMs, with an average change in rainfall-runoff erosivity of about 14.1%, 19%, and 24.2% for the 2030s, 2050s, and 2070s respectively. There was a concomitant increase in soil loss of 12.2%, 19.3% and 20.6% from the baseline for the 2030s, 2050s, and 2070s respectively. Though the combined average annual rainfall and erosivity show steady increases, some of the models (GFDLCM3-2.6 and HADCM2-2.6) reveal a likely decrease in annual rainfall and erosivity for the 2070s. Higher precipitation amounts were the major drivers of increasing spatial and temporal rainfall-runoff erosivity. More studies should be performed to include other important factors that exacerbate increases in erosivity, especially future changes in land use.

1. Introduction

Intense soil erosion arising from increasing rainfall-runoff erosivity is a critical issue in many basins around the globe (Angulo-Martínez and Beguería, 2012; Mondal et al., 2016; Vrieling et al., 2014). Rainfall-runoff erosivity relates to the climatic parameter of rainfall (Yang et al., 2003), and the powerful kinetic energy of falling raindrops often detach

soil particles and transport them together with surface runoff. This phenomenon has been demonstrated by Wischmeier (1968) with a raindrops-particle detachment relationship proposed by Govers (1991) that became the most commonly used index for quantifying rainfall erosivity as presented in the Universal Soil Loss Equation (USLE) (Wischmeier and Smith, 1978) or its revised-RUSLE (Renard, 1997). Erosivity does not have a linear relationship with soil erosion, as

* Corresponding author at: State Key Laboratory of Desert and Oasis Ecology, Xinjiang Institute of Ecology and Geography, Chinese Academy of Sciences, 818 South Beijing Road, Urumqi 830011, Xinjiang, China.

E-mail address: lilh@ms.xjb.ac.cn (L. Li).

<https://doi.org/10.1016/j.catena.2018.09.003>

Received 12 October 2017; Received in revised form 17 August 2018; Accepted 2 September 2018

Available online 07 September 2018

0341-8162/ © 2018 Elsevier B.V. All rights reserved.

erosion largely depends on raindrops, rainfall intensity, and duration (Salles et al., 2002). High-magnitude rainstorm events have some degree of control over rainfall erosivity (González-Hidalgo et al., 2009) and may increase with high rainfall intensities. Doetterl et al. (2012) reported that rainfall erosivity together with slope gradient explains about 75% of soil erosion variability. These factors represent triggers for runoff and soil erosion due to changes in precipitation.

Climate change may determine the nature of rainfall through the alteration of trends and patterns in rainfall in sub-Saharan Africa (Serdeczny et al., 2017), especially in the Niger basin area (Badou et al., 2017; Oyerinde et al., 2015). The climatic parameter of rainfall has been used to detect trends in rainfall-runoff erosivity using past and future climatic data in many basins (Gupta and Kumar, 2017; Panagos et al., 2017) and also in various sub-basins of the Lower Niger Basin (Fagbohun et al., 2016; Salako, 2010; Salako et al., 1995). Quantifying the effects of past and future climate-induced rainfall-runoff erosivity is essential in identifying key areas prone to erosion under a changing climate in West Africa, especially in the lower Niger Basin.

The mean precipitation change over West Africa shows a less evident trend and mostly oscillates between –10 and 10% where changes in climate cause more precipitation variability with greater amplitudes (Sylla et al., 2016). According to (IPCC, 2013), the range of precipitation trend varies from negative to positive values (mostly between –30 and 30%), indicating that projected precipitation is highly uncertain over the region. This uncertainty increases correspondingly with Representative Concentration Pathways (RCPs) forcing with the highest one found in the Sahel area. From a spatial perspective, most of West Africa experiences no changes, and a significant precipitation decrease of about 5–40% prevails in the West Sahel for the RCP4.5 to RCP8.5 and the time period shifts from 2036–2065 to 2071–2100 (Sylla et al., 2016). It fluctuates, and further experiences increase below the West Sahelian zone. These precipitation characteristics are controlled by the migration of a tropical frontal system, the Inter-Tropical Convergence Zone (ITCZ), a band of clouds over the tropics formed by the convergence of humid southeast trade winds and the dry Northeast trade winds (Oyerinde et al., 2016).

The use of GCMs has revealed that changes in rainfall patterns will impact soil erosion through several pathways, including changes in rainfall-runoff erosivity (Plangoen et al., 2013). Several studies have investigated, in isolation, changes in erosivity (Almagro et al., 2017; Plangoen and Babel, 2014), and a combined study of erosivity and soil erosion (Maeda et al., 2010; Segura et al., 2014) in different parts of the world using GCMs. Changes in erosivity have been directly linked to climate change effects on soil erosion (Nearing, 2001) because erosivity rates are expected to change in response to climate change.

Globally, rainfall patterns vary in time and space with expected increases in rainfall amounts in the tropics and subtropics. Separate researches by Salako et al. (1995) and Fagbohun et al. (2016) have shown that the tropical climate like the lower Niger basin, with its high rainfall intensity, has the highest mean erosivity. Vrieling et al. (2014) have evaluated the importance of the spatial and temporal variability of rainfall erosivity across Africa using the *R* factor in the RUSLE. The power with which soil particles are detached and carried by rain can be determined by changes in erosivity due to increased rainfall. Since a relationship has been established between rainfall characteristics and erosivity, an understanding of the spatiotemporal variability of rainfall erosivity is important. Thus, it is of significance to decipher whether the decreasing or increasing trend in rainfall amounts (climate change), for past and future climates in the Lower Niger Basin (LNB), will have any implication for rainfall erosivity.

Climate change is expected to impact erosivity in the LNB and other parts of the world. Temporal and spatial prediction of future rainfall-runoff erosivity under a changing climate has not been well documented in the LNB. The evaluation of rainfall erosivity and its implications can help practitioners and scientists to formulate better soil conservation practices and improve dam construction and agricultural

management. The outcome of this kind of research is generic and may reflect the kind of changes to be expected in other parts of the globe (e.g., the tropics and subtropics) and not necessarily confined to the study area. Therefore, the objectives of this study were to (i) quantify the nature of spatial and temporal variability of erosivity from rainfall amount using World climate data¹ and predicted rainfall from different GCMs (GFDLCM3, HADCM2, MIROC5, and MPIESMLR) for RCP 2.6 and 8.5 scenarios respectively, and (ii) evaluate the implications of changes in rainfall-runoff erosivity using RUSLE.

2. Site description

With a length of 4200 km, the Niger Basin houses the third longest river in Africa—the River Niger. It stretches from the mountains of Guinea through the Sahara Desert to the Gulf of Guinea, and is located between Longitude 11°30' W and 15° 00' E and Latitude 22°00' N and 5°00' N. The basin occupies areas with different climatic characteristics and is divided into four sub-basins based on differing hydrological and topographical features: the Upper, the Central Delta, the Middle and the Lower Niger Basins. The present research concentrates on the Lower Niger Basins. It covers about 528,000 km²: 81% in Nigeria, 12% in Cameroon and 7% in the Benin Republic. The basin is located in different ecological zones, passing through the Savannas (Sudan, Guinea, Derived), to the Humid forest and then the Freshwater forest, where the river flows into the Atlantic Ocean via a deltaic mouth. Rainfall varies spatially (Fig. 1a) within the basin with mean annual rainfall decreasing from south to north averaging 750 mm to over 2000 mm. Temperature is generally hot all-year-round, ranging from 25 °C to 32 °C, and the mean annual temperature range increases from 2.5 °C in the south of the basin, along the coast, to nearly 10 °C in the north, at the fringes of the Sahara Desert. Agriculture is the main source of livelihood, and it is predominantly rain-fed.

3. Materials and methods

3.1. Global climate data

Compared to the CMIP3, the CMIP5 is a significant model improvement and utilises a new set of emission scenarios referred to as RCPs. Global climate data from 4 GCMs (Table 1) under the RCP2.6 and RCP8.5 scenarios were used (Taylor et al., 2012) in this study. The GCMs were selected because of their (a) relative independence and good performance in precipitation simulation (Yan et al., 2015); (b) representativeness of the broader range of models and (c) satisfactory performance for the African continent (McSweeney et al., 2015). In the evaluation of future changes in rainfall erosivity and possible implications, projected climate data (precipitation), for the 2030s (2020–2039), 2050s (2040–2069), and 2070s (2060–2099) were obtained from the Climate Change Agriculture and Food Security (CCAFS)² portal. The data were statistically downscaled to a 30 arc-second (1 km²) horizontal resolution using the delta method (Ramirez-Villegas and Jarvis, 2010). The delta data, with respect to the baseline climate, WorldClim 2.0, were used to derive daily and monthly precipitation. Anomalies were then interpolated using a thin plate spline interpolation technique (Ramirez-Villegas and Jarvis, 2010). These datasets, for monthly precipitation, were used as input data for this research.

3.2. Changes in rainfall-runoff erosivity

To better understand the implications of changes in the rainfall-runoff erosivity, the *R* factor from the Revised Universal Soil Loss

¹ World Climate data, <http://worldclim.org/version2>, Accessed July 2017.

² GCMs, <http://www.ccafs-climate.org/data/>, Accessed July 2017.

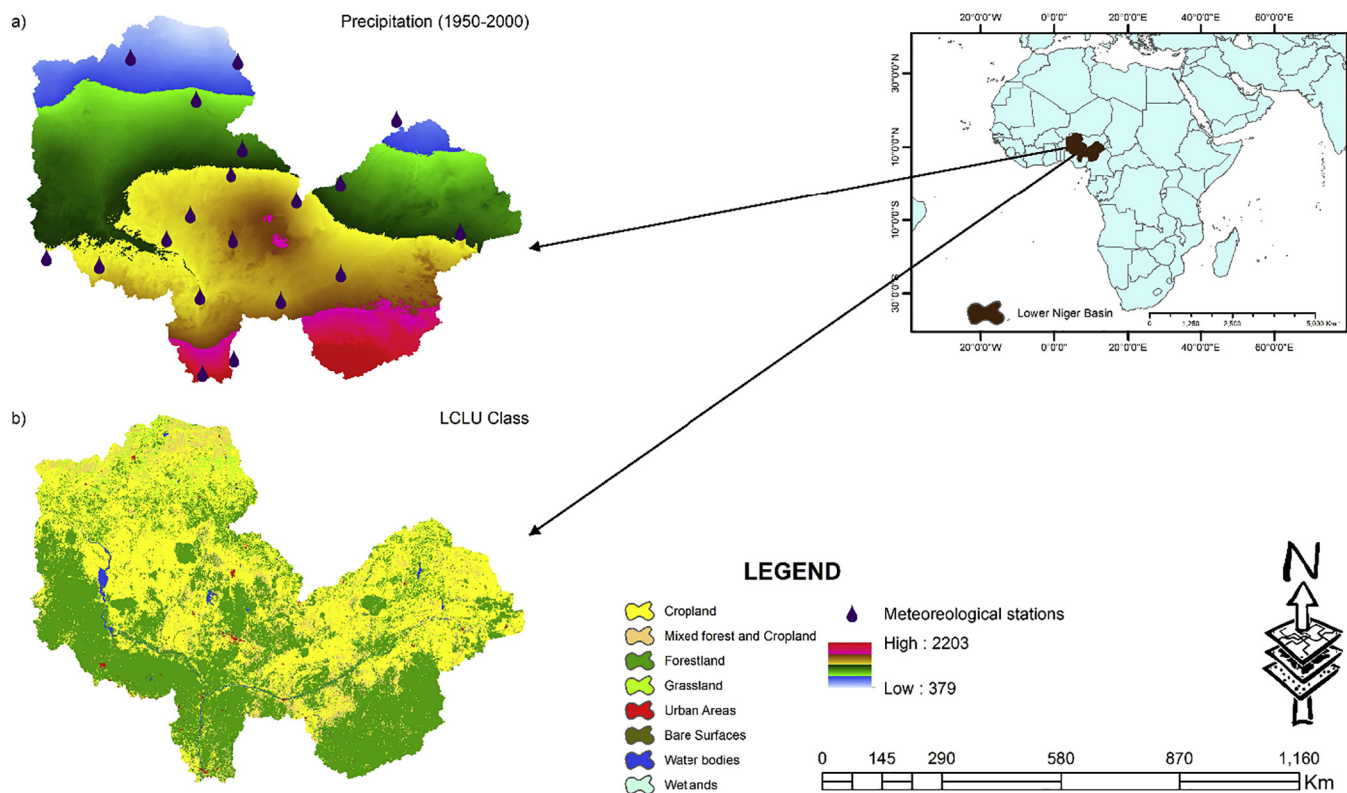


Fig. 1. Study area (a) average annual precipitation 1950–2000 from world climate data (b) Land cover and land use (LCLU) classes.

Table 1
Global Climate Models (GCMs).

Model	Abbreviation	Institution
GFDLCM3 (RCP 2.6)	GFDLCM3-2.6	Geophysical Fluid Dynamics
GFDLCM3 (RCP 8.5)	GFDLCM3-8.5	Laboratory, NOAA
HADCM2 (RCP 2.6)	HADCM2-2.6	Met Office Centre, UK
HADCM2 (RCP 8.5)	HADCM2-8.5	
MIROC5 (RCP 2.6)	MIROC5-2.6	CCSR/NIES/FRCGC, Japan
MIROC5 (RCP 8.5)	MIROC5-8.5	
MPiESMLR (RCP 2.6)	MPiESMLR-2.6	Max Planck Institute for Meteorology,
MPiESMLR (RCP 8.5)	MPiESMLR-8.5	Germany

Equation (RUSLE) was used based on several criteria as described in the equation:

$$A_{ij} = R_{ij} * K_{ij} * LS_{ij} * C_{ij} * P_{ij} \quad (1)$$

where A is the annual computed soil loss per unit area ($\text{ton ha}^{-1} \text{y}^{-1}$), of the grid located at (i, j) ; R is the rainfall-runoff erosivity factor ($\text{MJ mm ha}^{-1} \text{h}^{-1} \text{y}^{-1}$); K is the soil erodibility factor ($\text{ton ha MJ}^{-1} \text{mm}^{-1}$); LS is the average topographical parameter, L is the slope length factor, S is the slope gradient factor; C is the cover and management factor; and P is support practice factor (Renard, 1997).

To understand how changes in rainfall-runoff erosivity due to climate change affect soil erosion, rainfall-runoff erosivity was calculated using the precipitation values of the gridded GCMs comparing it with World climate (1950–2000).

3.2.1. Rainfall-runoff erosivity (R)

The derivation of R has been proposed using the modified Fournier index (F) (Arnoldus, 1977; Fournier, 1960) or average annual precipitation (P) (Nearing, 2001; Renard and Freimund, 1994) when only monthly precipitation data is available. In the tropics, the conversion of the Fournier index may give a spurious result (Salako, 2010). Therefore rainfall-runoff has been determined using the average annual

precipitation as derived by Renard and Freimund (1994).

$$R = 0.04830P^{1.610} \quad (P < 850) \quad (2)$$

$$R = 587.8 - 1.219P + 0.004105P^2 \quad (P > 850) \quad (3)$$

where R is rainfall-runoff erosivity and P is the average annual precipitation. They recommended using Eq. (2) when P is < 850 mm and Eq. (3) when P is > 850 mm.

The data used to derive R is gridded world climate data (hereafter referred to as baseline climate) of precipitation and the GCMs. It is more coherent to use the world climate data as the current climate (baseline) since the output of the four GCMs used in this study is bias-corrected based on the baseline climate data.

3.2.2. Soil erodibility (K factor)

Soil erodibility was estimated using soil properties compiled by Food and Agricultural Organisation (FAO, 1998)³ with Eq. (4) as used by Yang et al. (2003). The soil map is developed with a 5-min resolution using the FAO/UNESCO soil classification for the topsoil (0–30 cm).

$$K = \frac{1}{7.6} \left\{ 0.2 + 0.3 \exp \left[-0.0256 \text{SAN} \left(1 - \frac{\text{SIL}}{100} \right) \right] \right\} \left(\frac{\text{SIL}}{\text{CLA} + \text{SIL}} \right)^{0.3} \left(1 - \frac{0.25\text{OM}}{\text{Org} + \exp(3.72 - 2.95\text{OM})} \right) \left(1.0 - \frac{0.75\text{SN}}{\text{SN} + \exp(-5.51 + 22.9\text{SN})} \right) \quad (4)$$

where $\text{SN} = 1.0 \text{ SAN}/100$ and SAN , SIL , CLA , and OM are percentage content of sand, silt, clay and organic matter, respectively.

3.2.3. Topographic factor (LS)

LS factor was estimated from the Shuttle Radar Topography Mission (SRTM), 30 m resolution provided by the National Aeronautics and

³ Soil data; <http://www.fao.org/geonetwork/srv/en/metadata.show?id=14116>, Accessed August 2017.

Space Administration (NASA).⁴ It was derived using the algorithm in Eqs. (5) and (6). See Lebel et al. (2000) for a detailed description of the equation.

$$L_{i,j} = \frac{(A_{i,j-in} + D^2)^{m+1} - A_{i,j-in}^{m+1}}{D^{m+2} \cdot x_{i,j}^m \cdot (22.13)^m} \quad (5)$$

$$S_{i,j} = \begin{cases} 10.8 \sin \theta_{i,j} + 0.03, & \tan \theta_{i,j} < 9\% \\ 16.8 \sin \theta_{i,j} + 0.50, & \tan \theta_{i,j} \geq 9\% \end{cases} \quad (6)$$

3.2.4. Cover management factor (C factor)

In this study, the vegetation index derived from remote sensing data, such as NDVI, was used to account for the variation in vegetation density and condition (Reusing et al., 2000). MODIS biweekly mean NDVI provided by the National Aeronautics and Space Administration (NASA)⁵ for the rainy seasons (April–October 2016) computed with Eq. (7) (Zhou et al., 2008) for C factor, was used in this study.

$$C = \exp \left[-\alpha \frac{\text{NDVI}}{\beta - \text{NDVI}} \right] \quad (7)$$

where $\alpha = 2$ and $\beta = 1$ are unitless parameters that determine the shape of the curve relating to NDVI (NDVI-C curve) (Gupta and Kumar, 2017).

3.2.5. Support practice (P factor)

The study area has no major erosion support practices used, the P-factor (Table 2) was then assigned based on different types of land cover as given by Yang et al. (2003). The LCLU was observed and verified for proper classification during a field survey (carried out during the rainy season, between June and August 2017), and this information was used to classify the LCLU in the area adequately, and the P values were assigned accordingly.

To identify the area that is most affected by changes in past and future rainfall-runoff erosivity with regards to soil erosion, R, K, LS, C, and P factors have been multiplied using the R factor of different time periods. All data were resampled to a 1 km cell size of the gridded GCMs before use in RUSLE calculation in ArcGIS 10.4 environment.

3.2.6. Model validation

The validity of the derivation of R based on the data used was derived from mean monthly rainfall and average annual precipitation (1970–2013). The data (hereafter referred to as observation data) from 20 meteorological stations were collected from the Nigerian Meteorological Agency (NIMET). Using the coordinates of these stations, precipitation (mm) from the baseline climate data (1950–2000) and those of observation data were transferred to R statistical package to calculate the Rainfall-runoff erosivity for each of the datasets. The validity was statistically determined using the erosivity values of the baseline and observation data respectively in the hdroGOF package of R language.

The performance of the rainfall-runoff erosivity model was assessed by comparing the R of observation data (from 20 meteorological stations) with that of the base data using three measures: the root mean square error (RMSE), Nash-Sutcliffe coefficient (NASH), and Correlation Coefficient (CC). It is referred to Nash and Sutcliffe (1970) and Mondal et al. (2016) for a detailed description of these methods. The calculated RMSE values will have the same units as the R values. A small RMSE value indicates less discrepancy within the observed and predicted series, and therefore provides better accuracy in prediction. NASH values range from $-\infty$ to 1. Between observed and predicted rain-runoff erosivity, the value of 1 means a perfect match. The CC is

Table 2

P values assigned to various land use/land cover types.

LU/LC types	P-factor, Yang et al. (2003)	Area (ha)	Area (%)
Cropland	0.5	25,233,439	42.91
Forestland	1	25,103,383	42.69
Grassland	1	1,052,273	1.79
Mixed forest and cropland	0.8	6,666,963	11.34
Urban areas	1	202,459	0.35
Bare surfaces	1	11,275	0.019
Water bodies	1	521,587	0.887
Wetland	1	12,087	0.021

+1 in the case of a perfect increasing linear relationship, and -1 in case of a decreasing linear relationship. NASH and CC with higher values indicate better predictive accuracy. Furthermore, annual soil erosion (A) was compared with results obtained from existing literature in order to ascertain the level of accuracy of soil erosion derived from RUSLE.

4. Results

4.1. Rainfall-runoff erosivity under past and future climate

Simulated (world climate) and observed precipitation (1970–2013) were statistically and visually compared to summarise the strength with which the simulated world climate data (1950–2000) can reproduce the spatial pattern of mean and annual precipitation (Fig. S1, Tables S2 & 3). Taylor diagram (Fig. 2) was used to demonstrate the quality of the stimulated against the observed dataset for all the 20 stations. A correlation coefficient of about 0.99, and a similar standard deviation (1.0) between simulated and observed monthly precipitation was found (Table S1, Code S1). This shows that the simulated baseline precipitation reproduces past observed precipitation with considerable accuracy. Table 3 shows the rainfall-runoff erosivity (R) for the observation data for the 20 meteorological stations and the R-factor for the baseline data in the stations (Table S2).

Average annual R for the observation data ranges from 1345 to 12,609 $\text{Mj}\cdot\text{mm}\cdot\text{ha}^{-1}\text{h}^{-1}\text{yr}^{-1}$ for Katsina and Onitsha stations respectively (Table 3). The baseline data shows an R range of 1351–12,593 $\text{Mj}\cdot\text{mm}\cdot\text{ha}^{-1}\text{h}^{-1}\text{yr}^{-1}$ in Katsina and Onitsha stations respectively. Smithen and Schulze (1982) have reported 12,800 $\text{Mj}\cdot\text{mm}\cdot\text{ha}^{-1}\text{h}^{-1}\text{yr}^{-1}$ rainfall-runoff erosivity in Enugu (Nsuka), similar to the result of this study. Table 3 exemplifies the validation between the Rainfall-runoff erosivity derived from the observation data and that determined from the base data. The comparison of the values between R_{observed} and R_{baseline} yielded 0.97, 613.4 $\text{Mj}\cdot\text{mm}\cdot\text{ha}^{-1}\text{h}^{-1}\text{yr}^{-1}$ and 0.95 for CC, RMSE, and NASH respectively, indicating a good model performance for predicting rainfall-runoff erosivity for the past and future climate.

The predicted annual rainfall erosivity values from the four GCM projections were compared with those calculated using the gridded monthly rainfall data from World climate for the baseline period (1950–2000). Rainfall erosivity values derived from the four GCMs member ensembles vary across the RCP 2.6 and 8.5 (Table 4) compared with the results from the gridded baseline data. The result did not show a particular trend with regards to increase or decrease as the time period increases; rather it is synonymous with the trend in average annual precipitation where a reduction in average annual precipitation shows a reduction in average annual rainfall-runoff erosivity within the basin and vice versa. For instance, GFDL3 RCP 2.6 and 8.5 scenarios for all time slices show a more significant temporal variation of rainfall-runoff erosivity when the average annual precipitation is high. The MIROC5 for the both RCPs show a higher rainfall-runoff erosivity probably because of the high predicted spatial variation in precipitation with this ensemble. Spatially, for all the GCMs and baseline climate, the

⁴ DEM, <http://www.dwtkns.com/srtm30m/>, Accessed August 2017.

⁵ NDVI, <http://landsweb.nascom.nasa.gov/data/html>, Accessed June 2017.

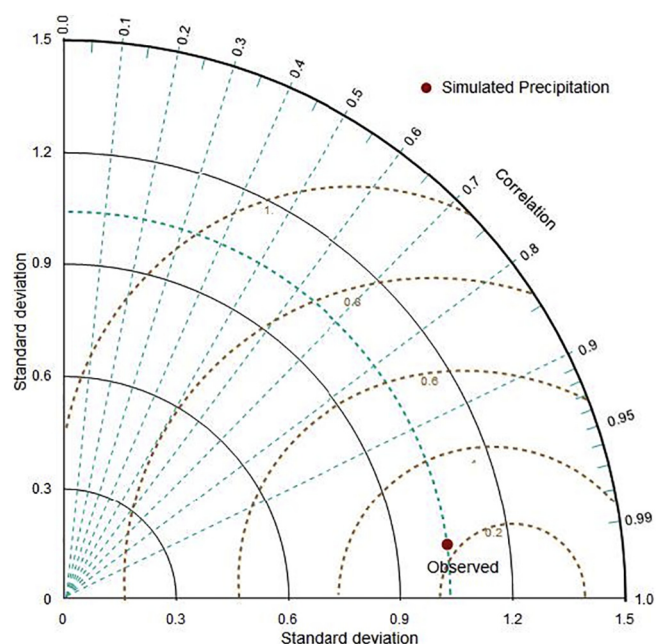


Fig. 2. Taylor Diagram for Precipitation.

Table 3

Rainfall-runoff erosivity for baseline and observation data.

Baseline data (1950–2000)				Observation data (1970–2013)			
Yelwa	3998	Bida	4756	Yelwa	3244	Bida	4616
Sokoto	1359	Minna	5114	Sokoto	1590	Minna	5234
Gusau	2365	Abuja	6542	Gusau	2953	Abuja	7048
Kaduna	5062	Jos	5388	Kaduna	5047	Jos	5614
Katsina	1351	Ibi	5837	Katsina	1345	Ibi	3982
Zaria	3775	Yola	3998	Zaria	4072	Yola	2744
Bauchi	3935	Lokoja	4840	Bauchi	3837	Lokoja	5818
Pokistum	1505	Onitsha	12,593	Pokistum	1653	Onitsha	12,609
Ilorin	4689	Enugu	11,039	Ilorin	4934	Enugu	11,098
Shaki	4623	Makurdi	6093	Shaki	4814	Makurdi	5146
Validation		CC		RMSE		NASH	
		0.97		613.4		0.95	

NB: R for baseline and observation data are measured in $\text{Mj}\cdot\text{mm}\cdot\text{ha}^{-1}\cdot\text{h}^{-1}\cdot\text{yr}^{-1}$ including the RMSE value.

rainfall-runoff erosivity is higher to the south of the basin but lower to the north of the basin.

Table 4 shows the impact of precipitation on past and future rainfall-runoff erosivity in the LNB and subsequently on soil erosion. The GCM ensembles show that precipitation and rainfall-runoff erosivity increase significantly from the baseline across all the ensembles. The average of all the ensembles reveals that precipitation increased during the 2030s, 2050s and 2070s to 1593 mm, 1630 mm and 1652 mm respectively from the baseline (1482 mm). However, the MIROC5 (the 2070s, RCP 2.6) has projected a higher rise in precipitation than the rest of the ensembles with the same scenario and period. There is also an average increase in rainfall-runoff erosivity for the 2030s, 2050s and 2070s of about 4806, 4983 and 5211 $\text{Mj}\cdot\text{mm}\cdot\text{ha}^{-1}\cdot\text{h}^{-1}\cdot\text{yr}^{-1}$ respectively.

Precipitation and erosivity vary across individual GCM without showing a steady increase or decline, while the average annual precipitation and erosivity shows a steady rise across all the ensembles put together (Table 4). Even though the average annual rainfall and erosivity show steady increases in all the climate models combined from the baseline climate, some of the models (GFDLCM3-2.6 and MPIESMLR-8.5) reveal a likely decrease in annual rainfall and erosivity in the 2030s and 2050s. The outcome of this research, as it relates to rainfall and erosivity patterns, has shown some similarities with other research

in tropical areas (with similar climate characteristics) of Brazil (Almagro et al., 2017) and Thailand (Plangoen and Babel, 2014), for past and future climate and for historical climate records within the LNB (Ezemonye and Emeribe, 2012; Fagbohun et al., 2016; Salako, 2010). In these studies, an increase in annual rainfall amount led to increase in erosivity and vice versa. Though this is not entirely true for all the ensembles, the MPIESMLR model, with a slight decrease in rainfall, shows an unusual spatial rainfall characteristic (Fig. 3) with higher erosivity (Table 4).

4.2. The RUSLE factors

The average annual rainfall erosivity factor (R) for the baseline station (1950–2000) was found to range from 715.5 in the North to 17,824.8 $\text{Mj}\cdot\text{mm}\cdot\text{ha}^{-1}\cdot\text{h}^{-1}\cdot\text{yr}^{-1}$ in the South (Fig. 4a). The highest value of the annual R factor was observed in the southern part of the basin (17,824.8 $\text{Mj}\cdot\text{mm}\cdot\text{ha}^{-1}\cdot\text{h}^{-1}\cdot\text{yr}^{-1}$), with medium values at the central areas of the basin, and decreasing northwards where the lowest values were observed (715.5 $\text{Mj}\cdot\text{mm}\cdot\text{ha}^{-1}\cdot\text{h}^{-1}\cdot\text{yr}^{-1}$). Using the station observation data as a case in point (Table 3), the values gradually increased towards the southern parts of the basin (e.g. Onitsha and Enugu) and reduced to the northern parts (Katsina and Sokoto). The spatial distribution of R values varied consistently with annual precipitation across the basin. This outcome is consistent with reports

made by Salako (2010) within the same research basin.

The soil erodibility factor (Fig. 4b) in the study area varies from 0 to 0.021, where 0 represents water surfaces. The soils in the basin are rich in sand (49.262%) and clay (32.2%), with very little organic matter content. Soils with a high proportion of organic matter content within the basin are considered to play a vital role in reducing soil erodibility.

Analysis of the landscape reveals that soil erodibility was highest in cropland (0.02) followed by forestland. The average soil organic matter content was found to be higher on low to moderate slopes but lower in steep slopes. The LS factor (Fig. 4c) in the present study varies from 0.0 to 41. The spatial distribution of the LS factor values are closely tied to slope categories (0° – 15° , 15° – 35° and $> 35^{\circ}$) and high elevation exceeding 1280 m. Higher LS values represent high susceptibility to soil erosion. The study area is majorly covered with cropland (42.91%), forestland (42.69%), mixed forest and cropland (11.34%) and Grassland (1.79%). Low C factor values were found in dense forest and increased progressively in cropland and grassland, and then to other land-uses, ranging from 2.8×10^{-7} to 1.32 (Fig. 4d). P factor ranged from 0.5 to 1 corresponding to different land-use as outlined in Table 2.

4.3. Implication of changes in past and future rainfall-runoff erosivity

The implication of change in erosivity as a result of past and future

Table 4

Changes in average annual rainfall-runoff erosivity and erosion under past and future climate change averaged across the basin.

Climate models	Precipitation	Rainfall erosivity ($\text{Mj}\cdot\text{mm}\cdot\text{ha}^{-1}\cdot\text{h}^{-1}\cdot\text{yr}^{-1}$)	Change (%)	Average erosion ($\text{t}\cdot\text{ha}^{-1}\cdot\text{yr}^{-1}$)	Change (%)
Base line	1482	9270	0	1272.5	0
2020–2039					
GFDLCM3-2.6	1603	10,728	15.7	1541.6	21.4
GFDLCM3-8.5	1379	7788	–15.9	1083.4	–14.9
HADCM2-2.6	1663	11,593	25.1	1476.9	16.1
HADCM2-8.5	1658	11,507	24.1	1465.4	15.2
MIROC5-2.6	1631	10,229	10.4	1692.4	32.9
MIROC5-8.5	1624	9976	7.6	1626.2	27.8
MPIESMLR-2.6	1573	11,151	20.3	1283.9	0.89
MPIESMLR-8.5	1614	11,656	25.7	1256.4	–1.27
Average		10,579	14.1*	1428.3	12.2*
2040–2069					
GFDLCM3-2.6	1611	10,870	17.3	1531.5	20.3
GFDLCM3-8.5	1603	10,601	14.4	1508.7	18.6
HADCM2-2.6	1628	11,063	19.3	1413.8	11.1
HADCM2-8.5	1650	11,380	22.8	1422.8	11.8
MIROC5-2.6	1627	10,202	10.1	1845.2	45
MIROC5-8.5	1691	12,588	35.8	1404.7	10.4
MPIESMLR-2.6	1544	10,842	16.9	1254.2	–1.44
MPIESMLR-8.5	1685	10,711	15.5	1762.9	38.5
Average		11,032	19*	1517.9	19.3*
2060–2099					
GFDLCM3-2.6	1586	10,603	14.4	1453.7	14.2
GFDLCM3-8.5	1693	11,813	27.4	1767.2	38.9
HADCM2-2.6	1611	10,869	17.3	1377.4	8.2
HADCM2-8.5	1694	12,131	30.9	1487.7	16.9
MIROC5-2.6	1709	12,099	30.5	1771.3	39.2
MIROC5-8.5	1675	10,469	12.9	1899.1	49.2
MPIESMLR-2.6	1594	11,517	24.2	1330.6	4.7
MPIESMLR-8.5	1656	12,627	36.2	1191.3	–6.4
Average		11,516	24.2*	1534.8	20.6*

NB: Average* implies % change for the corresponding average values (erosivity and erosion) for all the GCMs from the baseline climate.

changes in climate is illustrated in Table 4, showing variation in potential annual soil loss for past climate and future scenarios. Increases in soil erosion reflecting variation in annual erosion are evident under all the scenarios, with the basin soil erosion showing significant increasing trend under all the scenarios except for the GFDLCM3-RCP8.5 (2020–2039). The GFDLCM3-RCP8.5 (2020–2039) shows a decline in rainfall-runoff erosivity of about –14.9% from the baseline climate, with rainfall-runoff erosivity increasing from the baseline by about 15.7% at the GFDLCM3-2.6 for the 2020–2039. The annual soil erosion also shows a corresponding increase of about 21.4% from the baseline climate for the same time slice and climate scenario. The MPIESMLR-8.5 also shows a decline in soil erosion (–1.27%) even though the erosivity is reported to be high. For the 2020 to 2039 climate period, the MIROC5-2.6 and MIROC5-8.5 show the highest positive percentage increases, in soil erosion, of about 32.9% and 27.8% respectively. As the rainfall-runoff erosivity increases from the baseline basin erosion, the percentage changes in annual basin erosion show increases. Similarly, for the 2040–2069 climate period, as baseline rainfall-runoff erosivity increased, the annual erosion increase. Within this climate period, the highest erosivity occurred at the MIROC5-8.5 which had an annual erosion of about $12,588\text{ t}\cdot\text{ha}^{-1}\cdot\text{yr}^{-1}$, increasing from the baseline rainfall-runoff erosivity by 35.8%. The highest annual erosion for this time period was observed in the MIROC5-2.6 with about 45% increase from the baseline erosion. The quantity of erosivity for this ensemble (MIROC5) is not directly synonymous with a corresponding increase in the soil erosion as compared to other GCMs. For instance, the MIROC5-8.5 reports the highest amount of erosivity yet has a low annual soil erosion of $1404.7\text{ t}\cdot\text{ha}^{-1}\cdot\text{yr}^{-1}$. The 2040–2069 time period also shows the lowest annual erosion at MPIESMLR-2.6 dropping by –1.44% from the baseline erosion.

For 2060 to 2099 climatic period, the MPIESMLR-8.5 showed the highest rainfall-runoff erosivity with a percentage rise of 36.2% from

the baseline. However, the average annual soil erosion also showed a decline (–6.4%) for this scenario. The HADCM2-2.6 and MIROC-8.5 showed a high soil erosion in relation with erosivity.

Overall, there is an increase in the mean annual erosion for most of the model ensembles from 2020–2039 through the 2060–2099 climate period respectively; signalling a potential increase in annual soil erosion under the future climatic scenarios. This agrees with the work conducted by Yang et al. (2003), where they reported global percentage rise in future soil erosion due to climate change with Africa reaching about 15.7% in the 2090s. Additionally, the individual GCMs do not show the same trend in annual soil erosion (Table 4). While most predicting an increasing trend in soil loss, the MPIESMLR shows a decreasing trend in some time slices. However, the GFDLCM3 shows a mixed trend for different time periods. de Hipt et al. (2018) assessed the impact of climate change on soil erosion in a catchment located in the upper Niger Basin in Burkina Faso. Their results showed that three models (RACMO-EARTH, CCLM-CNRM, HIRHAM-NorESM) predict an increase of about 14.1%–64.4% of soil erosion while two models (CCLM-ESM, CCLM-EARTH) forecast a decreasing trend (21.2%–45%) of soil erosion. The HIRHAM-EARTH model gave a mixed result. Fig. 5 illustrates the spatial variation in erosivity, and potential annual soil erosion for the LNB estimated from the RUSLE model under different future climatic scenarios from a combination of GFDLCM3, HADCM2, MIROC5 and MPIESMLR with RCP 2.6 and RCP 8.5 emission scenarios. The increases in annual soil erosion could be as a result of a combination of several factors, not least of which are changes in rainfall-runoff erosivity resulting from changes in annual rainfall.

Climate change influences on soil erosion may rise or decline depending on the changes in rainfall-runoff erosivity and other interacting factors (Plangoen et al., 2013), which is true of the LNB. The result of mean soil loss changes (Table 4) derived from the RUSLE model under the past and future climate change projections from a combination of

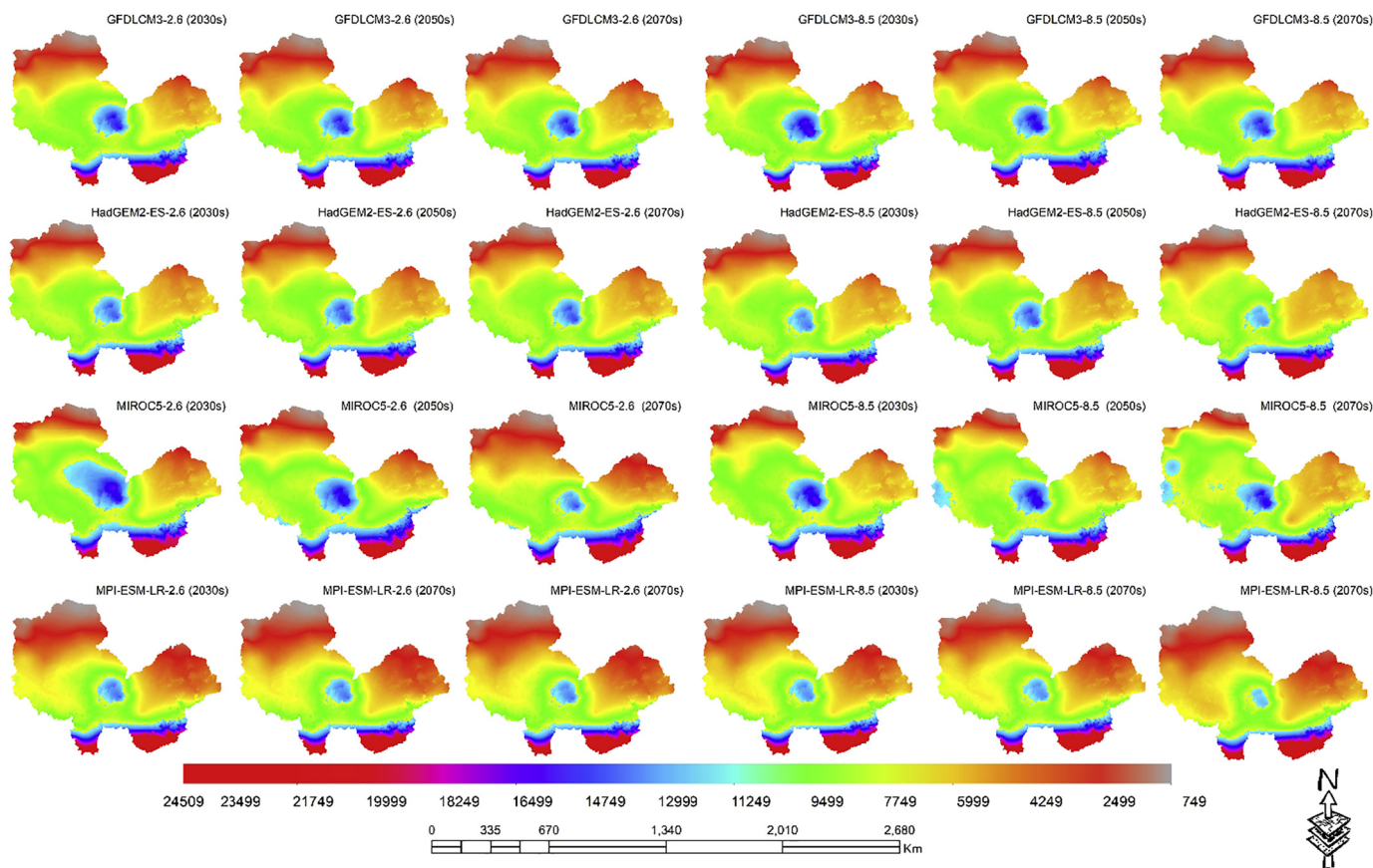


Fig. 3. Predicted annual mean rainfall erosivity in the future for RCPs 2.6 (left) and RCPs 8.5 (right) for different time slices for the GCM projections.

four different climate models for three different time periods are between $1428.3 \text{ t ha}^{-1} \text{ yr}^{-1}$ and $1534.8 \text{ t ha}^{-1} \text{ yr}^{-1}$ for 2020–2039 and 2060–2099 time periods respectively. There is no significant difference in the annual soil erosion result reported in this research (Fig. 5b) with that by other researchers within the LNB. For instance, Fagbohun et al. (2016) and Adediji et al. (2010) reported an annual soil erosion of 0 to > 2200 and 0.0 to $4185.12 \text{ t ha}^{-1} \text{ yr}^{-1}$ in Anambra basin and Katsina respectively. Similarly, Gadiga and Martins (1999) reported an average annual erosion of about $2381.87 \text{ t ha}^{-1} \text{ yr}^{-1}$ in the Upper Yedzaram Catchment of Mubi in Adamawa within the LNB. This outcome from other researchers has shown an explicit agreement and validates the annual erosion modelled with RUSLE in the study site.

5. Discussion

The impact of climate change on rainfall-runoff erosivity can be expressed by changes in total rainfall. The decrease in total precipitation and the indices representing rainfall aggressiveness should not be interpreted as a decrease in rainfall-runoff erosivity because the process of soil erosion is not only linked to rainfall-runoff erosivity but also to the dynamics of vegetation, soil properties, and surface geomorphology. Rapid forest disappearance or deterioration, especially due to population pressures and non-sustainable resource utilisation within the Niger basin (Chineke et al., 2011) could play a significant role in soil loss variation since erosivity rates vary across the study area. High altitude within the study area also accounts for erosivity amounts. Moderate rainfall erosivity characterises the North-central part (Figs. 3 & 5a) of the study area. The Jos Plateau with an average altitude of 1280 m, found in this region, has a higher rainfall compared to its surrounding lowland, and consequently higher erosivity. The surface characteristics of this area with regards to high slope play a significant role in soil loss increases in LNB (Fig. 5b).

The erosivity pattern observed in this study is due to the drier climate to the North (the Sudan Savanna) and the wetter Guinea Savanna in South of the basin. Average annual rainfall erosivity within the study area could exceed $40,000 \text{ MJ·mm·ha}^{-1} \text{ h}^{-1}$ (Salako, 2010), and this is due in part to the high rainfall intensities and amounts experienced in the south. This phenomenon of high erosivity is common in the humid tropics (Hoyos et al., 2005), which occupies a large part of the study area. The Guinea Savanna within the LNB has rainfall occurring for up to 7 months during the rainy season with $> 1200 \text{ mm}$ mean annual rainfall. Its Sudanian counterpart, on the other hand, has only 3–5 months of rainy season and an annual rainfall ranging from 200 to 800 mm. These figures imply that areas with high rainfall amounts are likely to have high annual erosivity (Table 3). Erosivity variation has also been reported by Ezemonye and Emeribe (2012) in their study in the southern part of LNB. They attributed rainfall seasons to erosivity where the dry season corresponds to low erosivity and vice versa. Additionally, nearness to the Gulf coast of the Atlantic which brings in rain-bearing Tropical Maritime air-mass may account for the high erosivity in the southern part of LNB. Also, urbanisation and industrialisation in the southern part may directly contribute to climate change induced by global warming resulting in rainfall increases and consequently erosivity. The result of this research agrees with the works of Salako (2008) and Ufoegbune et al. (2011) who reported high erosivity in the southern part of the study area. Ufoegbune et al. (2011) argued vehemently that climate change resulting from global warming, as a result of industrialisation, play a role in erosivity increases.

Erosivity will be influenced by variation in rainfall pattern and amount due to climate change. This could be caused by a reduction of rain-days and increase in rainfall intensities falling with erosive power during days of fewer rainfall as observed by Salako (2008) for the study area. Since rainfall is evidently high in most part of the LNB, variation in the pattern of erosivity is likely to follow the direction of rain

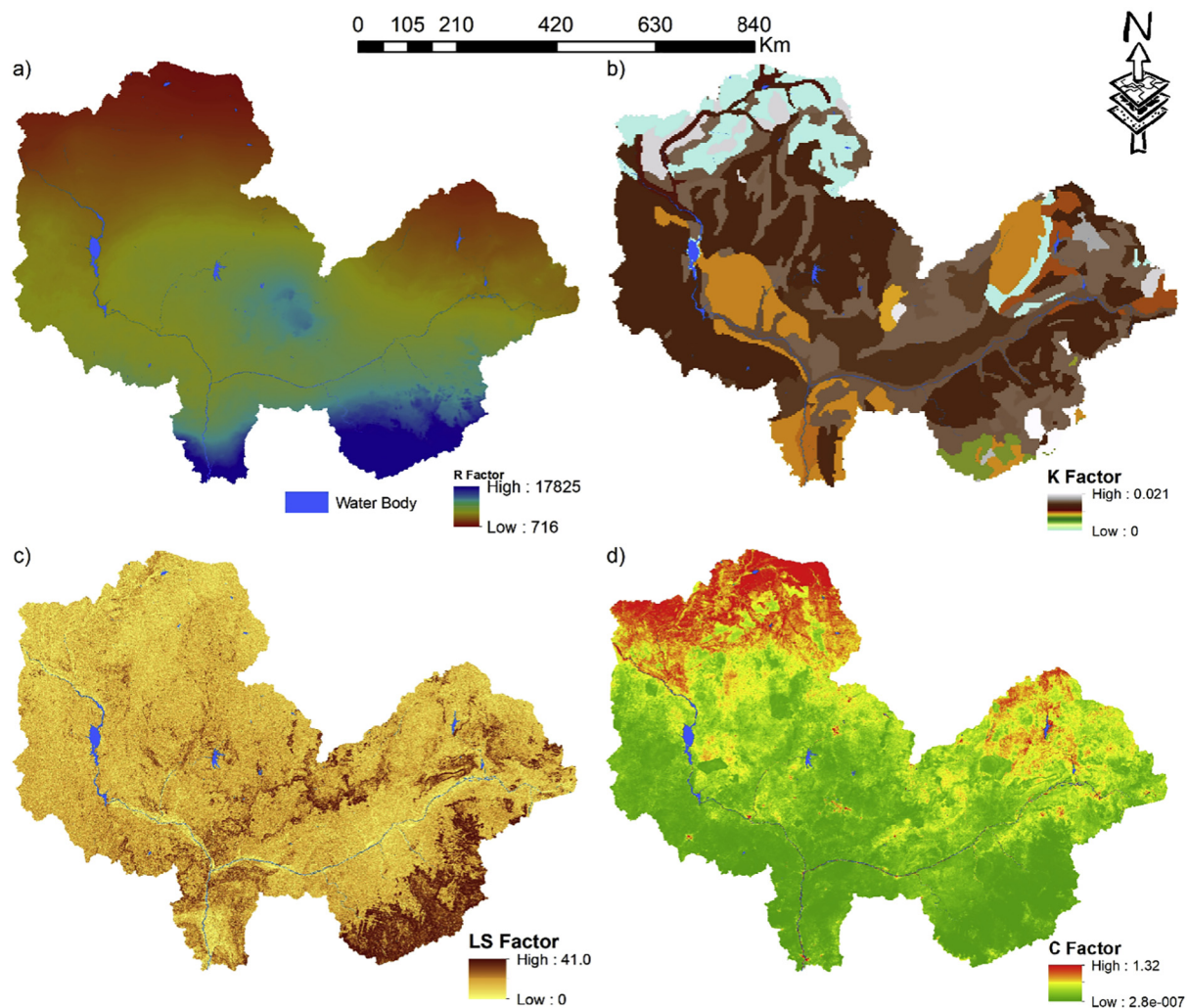


Fig. 4. RUSLE factors used to determine soil loss erosion (a) Rainfall-runoff erosivity (b) Soil erodibility factor (c) Length and Slope factor (d) Crop management factor.

intensities and amounts. Expected increases in rainfall across the West African Sahel are evident in CMIP5 climate projections (Klutse et al., 2016) as discovered in this research. Therefore, if future rainfall increases in intensities and amounts, rainfall erosivity will increase.

Studies in the tropics have projected substantial increase or decrease in erosivity for future climate. For instance, Almagro et al. (2017) discovered a decrease in the rainfall erosivity over the North, Northeast, Central-West and Southeast regions of Tropical Brazil and increase for the South region projected by HadGEM2-ES and MIROC5 for RCP 4.5 and 8.5 scenarios. These projections correspond to annual rainfall predicted in their study. They attributed this to be the consequences of the El Niño Southern Oscillation (ENSO). The current study also projected spatial increases and decreases in erosivity (Tables 3 & 4, Figs. 3 & 5) for the LNB in relation to the rainfall amount occurring in the area for different GCMs (for RCP 2.6 and 8.5 scenarios). However, this outcome is not as a result of ENSO but could be attributable to the southwest-northeast migration of the ITCZ in the study area. As the ITCZ migrates southwards, it draws in the moisture-laden Tropical Maritime air mass that moves to the fringes of the Sahara, which brings rain. It retreats rapidly down south as it comes under the influence of the Tropical Continental air mass which supplies little moisture for rainfall formation, resulting in a faster north-south movement (Odekunle, 2004). This phenomenon accounts for the spatial distribution of rainfall amounts within the study area and in turn, could explain why some areas have higher erosivity than others. The timing of the

ITCZ is also very important as rain formation is highly dependent on when moisture carrying air mass arrives. It has been argued, however, that the timing, amount and intensity of rainfall, rather than just the average annual precipitation amount, control the degree at which rainfall-runoff erosivity and by extension, erosion responds to changes in climate (Plangoen et al., 2013). Vrieling et al. (2014) have reported that seasonal change in Sub-Saharan Africa experiencing high rainfall-runoff erosivity is closely linked to the seasonal movement of ITCZ in Western Africa, implying that more erosivity power is expected in LNB. In general, the spatial variability of rainfall erosivity follows that of annual rainfall in LNB, reducing from south to north.

Maeda et al. (2010) used ECHAM5 for three greenhouse gas emission scenarios (SRA1B, SRA2, and SRB1) as a reference for perturbing precipitation into SRA1B, SRA2 and SRB1 scenarios for future erosivity simulation for Eastern Africa. They discovered that erosivity varied considerably across the different scenarios with no specific direction or magnitude, signifying lack of agreement between the simulated scenarios. They attributed this to uncertainties inherent in the GCMs. This is similarly true of the models used in this research as all the GCMs do not show the same direction or magnitude for erosivity, and can be attributed to the uncertainties related to the inability of the GCMs to capture, equally, the variability and characteristics of precipitation in the LNB. Also, the contrasting characteristics of the MIROC5 and MPIESMLR model may be attributed to the spatial uncertainty inherent in climate model.

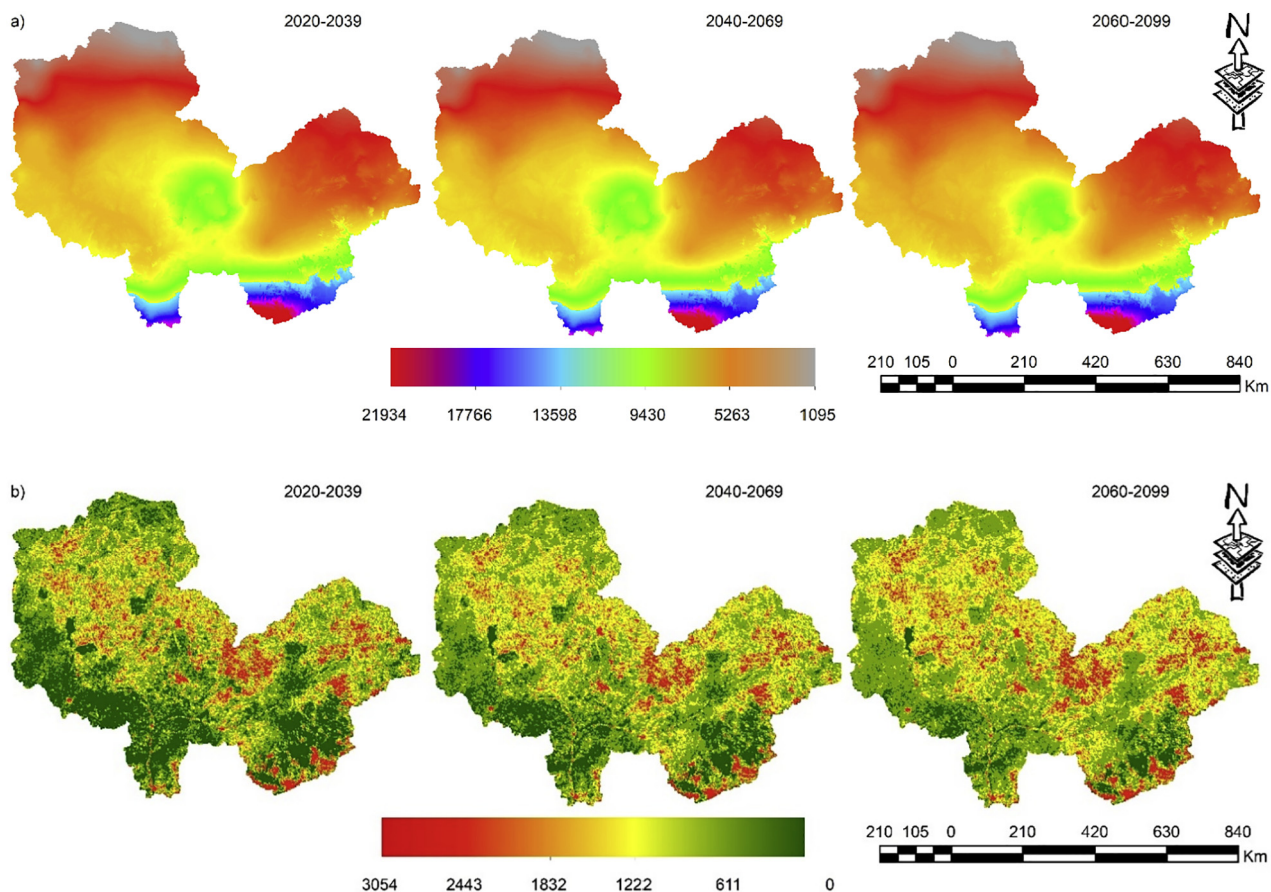


Fig. 5. Predicted Rainfall-runoff erosivity and soil loss under climate change: (a) Predicted rainfall runoff erosivity ($\text{Mj-mm-ha}^{-1} \text{h}^{-1} \text{yr}^{-1}$) under all the scenarios for different time slices and (b) Predicted future soil erosion ($\text{t ha}^{-1} \text{yr}^{-1}$) under all the scenarios for different time slices.

Meanwhile, [Segura et al. \(2014\)](#) evaluated the changes in rainfall-runoff erosivity, across the conterminous United States, under nine climatic projections for three emission scenarios (A2, A1B, and B1) and found that the values would increase with time according to all the projections considered between 1970 and 2090. Changes in the erosive power of rainfall in response to climate change may affect rainfall-runoff erosivity behaviour. It may also vary due to change in frequency and intensity of precipitation, temperature, and land use/land cover. It is therefore evident that future precipitation will intensify and the most influencing factor will be the power at which rainfall erodes soil. It has shown from the result that the power of rain is a very important factor that controls erosivity within the lower Niger basin. It is, therefore, pertinent to say that this outcome is not specific for this research area alone and may be generic for other tropical and subtropical areas.

The increases in estimated annual soil erosion in the LNB reflect a combination of factors with respect to the climatic scenarios used in this study. High soil loss is seen to occur in the extreme south and towards the North of the study site. These areas have steep slopes and are highly erodible soils where there is the possibility of deforestation and/or forest burning for agricultural activities. The Northern part (Figs. 4a & 5b), including northeast (NE), north-central (NC) and northwest (NW) of the study area, is popular sites for large-scale agricultural practices ([Chineke et al., 2011](#)), such as animal grazing which uncovers the topsoil, resulting to increased soil erosion observed in the region. It is obvious that there is an observed spatial increase (Fig. 5b) in annual soil erosion for the different time slices (2020s, 2050s, and 2070s). The current results for annual soil erosion (Table 4, Fig. 5) observed were as a result of non-uniform precipitation signal for individual GCMs. It, therefore, means that the increase or decrease in precipitation based on the GCM output determines annual soil erosion rates in LNB. Soil

erosion increases reported here is obviously related to the amount of rainfall. Though rainfall and erosivity are not usually linearly related to erosion as has been observed from some of the GCMs presented in Table 4. Higher rainfall and erosivity amount do not lead to higher annual erosion. This could be as a result of the characteristics of the rains in LNB. The rains often come in larger drops with high intensity during greater part of the rainy season, and the duration is often long at some period. Soil loss erosion is expected to rise as a result of an increase in annual precipitation and rainfall-runoff erosivity when the downscaled climate change projections are used in determining soil loss in LNB. [Fagbohun et al. \(2016\)](#), have reported an increase in soil erosion due to variation in rainfall and lack of erosion control practices in a sub-basin within the LNB. So, expected changes in rainfall behaviour may have a significant impact on soil erosion. Even when the study site shows that the combined percentage of cropland and mixed cropping is more than that of the forested area (Table 2), rainfall erosivity, which is not amenable to human modification, is a critical factor controlling soil erosion. Given that the study site does not have any major erosion support practice system, the impact of rainfall erosivity can be more severe because soils are easily eroded.

6. Uncertainties

To address uncertainties inherent to climate models, the use of multiple GCMs and corresponding scenarios are important for this study. These multiple GCMs used show non-uniformity in climate change signal (e.g., MIROC5 and MPIESMLR). [de Hipt et al. \(2018\)](#) has argued that disagreeing signals between models, in the upper part of the LNB in West Africa, may be attributed to data scarcity and limited knowledge of the regional climatology of the area. The downscaled

climate data set is entrenched in some degree of uncertainties. Therefore, the downscaling technique, Delta Change method, utilised as a part of this research may also contribute the degree of uncertainties.

High uncertainties in the magnitude of changes projected across the four downscaled GCMs were inherited from large inconsistencies linked with rainfall projections in West Africa. These could be credited to substantial divergence among the different observational datasets available over the region leading to variation in GCM products output (Oyerinde et al., 2016). The complexity of regional climates and the influence of regional geographic features, such as deserts, land cover variations, mountain chains, large lakes, land-sea contrasts, and sea surface temperatures of the surrounding oceans may also increase uncertainties (Sylla et al., 2016). These may have an actual or potential impact on modelled erosivity or soil erosion of the LNB since the rainfall data are monthly average at 1 km resolution. Also, the monthly rainfall may result in uncertainties since it does not capture intensities, size of raindrops and duration of effective rain which are linearly related to erosion. This impact could be an underestimation of erosivity in high erosive regions (e.g., Jos Plateaus and extreme south close to the Atlantic Ocean) due to high raindrops thereby increasing uncertainty and biases on the modelled erosivity and consequently on erosion. The biases may even be exacerbated because all the factors used for the derivation of the soil erosion were resampled to 1 km resolution. The effect of these uncertainties is considered not significant for the purpose of this study. Nonetheless, the importance of this type of research is not to portray an exact event but to offer a comprehensive understanding of the possible future scenarios for researchers and policymakers. It is suggested, however, that future research in the LNB area should seek for finer/higher resolution dataset to use in modelling erosivity and soil erosion.

7. Conclusion

As a sensitive basin responding to environmental change by climate, the LNB has experienced a recurrence of heavy precipitation events, more so in recent decades. Fluctuations in rainfall-runoff erosivity and soil erosion were unavoidable. Nevertheless, the limited and/or inadequate spatial spread of precipitation observation in this tropical latitude has restricted rainfall-runoff research and by extension soil erosion on a large scale. Little is known about the variations in rainfall-runoff erosivity for the entire basin. This research evaluated the long-term variations in the annual rainfall-runoff erosivity in the LNB utilising past and future climate data. The conclusions were as per the following:

- (1) Increasing trends in the annual rainfall-runoff erosivity were observed from the baseline climate up to the GCMs, and the climate scenarios experienced variations in both erosivity and soil loss. From the baseline climate, the average change in the percentage of rainfall-runoff erosivity is 14.1%, 19%, and 24.2% and 12.2%, 19.3% and 20.6% for soil erosion in the 2030s, 2050s, and 2070s respectively.
- (2) Though the combined average annual rainfall and erosivity for all the climatic models in all scenario shows steady increases from the baseline climate, some of the models (GFDLCM3-2.6 and HADCM2-2.6) reveal a likely decrease in annual rainfall and erosivity in the 2070s
- (3) Higher precipitation amounts were the major drivers of the increase in the spatial and temporal rainfall-runoff erosivity.
- (4) The relative increasing rate for erosivity and soil erosion are comparable, signalling a significant contribution of rainfall-runoff erosivity to the increase in soil erosion.

The outcome of this paper can be generic and may reflect the kind of changes experienced or expected in other tropical areas. Generally, wet climate increases the risk of soil erosion by increasing rainfall-runoff

erosivity in the lower Niger basin, and more studies should be performed to include other important factors that encourage future increases in erosivity, especially future changes in land use.

Supplementary data to this article can be found online at <https://doi.org/10.1016/j.catena.2018.09.003>.

Acknowledgement

We are grateful for the supports from the Strategic Priority Research Program of Chinese Academy of Sciences, Pan-Third Pole Environment Study for a Green Silk Road (Pan-TPE) (No. XDA2004030202), and the Chinese Academy of Science-the Third World Academy of science (CAS-TWAS) presidential fellowship for their financial support during the period of the fellowship that enabled the completion of this research. The authors are grateful to the supports in data collection and analysis from the CAS Research Centre for Ecology and Environment of Central Asia.

References

- Adediji, A., Tukur, A., Adepoju, K., 2010. Assessment of revised universal soil loss equation (RUSLE) in Katsina area, Katsina state of Nigeria using remote sensing (RS) and geographic information system (GIS). *Iran. J. Energy Environ.* 1 (3), 255–264.
- Almagro, A., Oliveira, P.T.S., Nearing, M.A., Hagemann, S., 2017. Projected climate change impacts in rainfall erosivity over Brazil. *Sci. Rep.* 7.
- Angulo-Martínez, M., Beguería, S., 2012. Trends in rainfall erosivity in NE Spain at annual, seasonal and daily scales, 1955–2006. *Hydrol. Earth Syst. Sci.* 16 (10), 3551.
- Arnoldus, H., 1977. Methodology used to determine the maximum potential average annual soil loss due to sheet and rill erosion in Morocco. In: *FAO Soils Bulletins*. FAO.
- Badou, D.F., Kapangaziwiri, E., Diekkrüger, B., Hounkpè, J., Afouda, A., 2017. Evaluation of recent hydro-climatic changes in four tributaries of the Niger River Basin (West Africa). *Hydrol. Sci. J.* 62 (5), 715–728.
- Chineke, T., Idinoba, M., Ajayi, O., 2011. Seasonal evapotranspiration signatures under a changing landscape and ecosystem management in Nigeria: implications for agriculture and food security. *Am. J. Sci. Ind. Res.* 2 (2), 191–200.
- Doetterl, S., Van Oost, K., Six, J., 2012. Towards constraining the magnitude of global agricultural sediment and soil organic carbon fluxes. *Earth Surf. Process. Landf.* 37 (6), 642–655.
- Ezemonye, M., Emeribe, C., 2012. Rainfall erosivity in southeastern Nigeria. *Ethiop. J. Environ. Stud. Manag.* 5 (2), 112–122.
- Fagbohun, B.J., Anifowose, A.Y., Odeyemi, C., Aladejana, O.O., Aladeboyeje, A.I., 2016. GIS-based estimation of soil erosion rates and identification of critical areas in Anambra sub-basin, Nigeria. *Model. Earth Syst. Environ.* 2 (3), 159.
- FAO, 1998. *Land and Water Digital Media Series N-1*. December. 92-5-104050-8.
- Fournier, F., 1960. *Climate and Erosion*. University of Paris, Paris.
- Gadiga, B.L., Martins, A.K., 1999. The Use of Revised Universal Soil Loss Equation (RUSLE) as a Potential Technique in Mapping Areas Vulnerable to Soil Erosion in the Upper Yedzaram Catchment of Mubi.
- González-Hidalgo, J., de Luis, M., Batalla, R., 2009. Effects of the largest daily events on total soil erosion by rainwater. An analysis of the USLE database. *Earth Surf. Process. Landf.* 34 (15), 2070–2077.
- Govers, G., 1991. Spatial and temporal variations in splash detachment: a field study. In: *Loess, Geomorphological Hazards and Processes*, Catena Supplement, pp. 15–24.
- Gupta, S., Kumar, S., 2017. Simulating climate change impact on soil erosion using RUSLE model – a case study in a watershed of mid-Himalayan landscape. *J. Earth Syst. Sci.* 126 (4), 43.
- de Hipt, F.O., et al., 2018. Modeling the impact of climate change on water resources and soil erosion in a tropical catchment in Burkina Faso, West Africa. *Catena* 163, 63–77.
- Hoyos, N., Waylen, P.R., Jaramillo, Á., 2005. Seasonal and spatial patterns of erosivity in a tropical watershed of the Colombian Andes. *J. Hydrol.* 314 (1), 177–191.
- IPCC, 2013. In: Stocker, T.F., et al. (Eds.), *Climate Change 2013: The Physical Science Basis*. Contribution of Working Group I to the Fifth Assessment Report of IPCC the Intergovernmental Panel on Climate Change. Cambridge University Press.
- Klutse, N.A.B., et al., 2016. Daily characteristics of West African summer monsoon precipitation in CORDEX simulations. *Theor. Appl. Climatol.* 123 (1–2), 369–386.
- Lebel, T., Delclaux, F., Le Barbé, L., Polcher, J., 2000. From GCM scales to hydrological scales: rainfall variability in West Africa. *Stoch. Env. Res. Risk A.* 14 (4), 275–295.
- Maeda, E.E., Pellikka, P.K., Siljander, M., Clark, B.J., 2010. Potential impacts of agricultural expansion and climate change on soil erosion in the Eastern Arc Mountains of Kenya. *Geomorphology* 123 (3–4), 279–289.
- McSweeney, C., Jones, R., Lee, R.W., Rowell, D., 2015. Selecting CMIP5 GCMs for downscaling over multiple regions. *Clim. Dyn.* 44 (11–12), 3237–3260.
- Mondal, A., Khare, D., Kundu, S., 2016. Change in rainfall erosivity in the past and future due to climate change in the central part of India. *Int. Soil Water Conserv. Res.* 4 (3), 186–194.
- Nash, J.E., Sutcliffe, J.V., 1970. River flow forecasting through conceptual models part I—a discussion of principles. *J. Hydrol.* 10 (3), 282–290.
- Nearing, M., 2001. Potential changes in rainfall erosivity in the US with climate change during the 21st century. *J. Soil Water Conserv.* 56 (3), 229–232.
- Odekunle, T., 2004. Rainfall and the length of the growing season in Nigeria. *Int. J.*

- Climatol. 24 (4), 467–479.
- Oyerinde, G.T., et al., 2015. Hydro-climatic changes in the Niger basin and consistency of local perceptions. *Reg. Environ. Chang.* 15 (8), 1627–1637.
- Oyerinde, G.T., et al., 2016. Quantifying uncertainties in modeling climate change impacts on hydropower production. *Climate* 4 (3), 34.
- Panagos, P., et al., 2017. Towards estimates of future rainfall erosivity in Europe based on REDES and WorldClim datasets. *J. Hydrol.* 548, 251–262.
- Plangoen, P., Babel, M., 2014. Projected rainfall erosivity changes under future climate in the Upper Nan Watershed, Thailand. *J. Earth Sci. Clim. Chang.* 5 (10), 1.
- Plangoen, P., Babel, M.S., Clemente, R.S., Shrestha, S., Tripathi, N.K., 2013. Simulating the impact of future land use and climate change on soil erosion and deposition in the Mae Nam Nan sub-catchment, Thailand. *Sustainability* 5 (8), 3244–3274.
- Ramirez-Villegas, J., Jarvis, A., 2010. Downscaling global circulation model outputs: the delta method decision and policy analysis Working Paper No. 1. *Policy Anal.* 1, 1–18.
- Renard, K.G., 1997. Predicting Soil Erosion by Water: A Guide to Conservation Planning with the Revised Universal Soil Loss Equation (RUSLE).
- Renard, K.G., Freimund, J.R., 1994. Using monthly precipitation data to estimate the R-factor in the revised USLE. *J. Hydrol.* 157 (1–4), 287–306.
- Reusing, M., Schneider, T., Ammer, U., 2000. Modelling soil loss rates in the Ethiopian Highlands by integration of high resolution MOMS-02/D2-stereo-data in a GIS. *Int. J. Remote Sens.* 21 (9), 1885–1896.
- Salako, F.K., 2008. Rainfall variability and kinetic energy in southern Nigeria. *Clim. Chang.* 86 (1), 151–164.
- Salako, F., 2010. Development of isoerodent maps for Nigeria from daily rainfall amount. *Geoderma* 156 (3), 372–378.
- Salako, F., Ghuman, B., Lal, R., 1995. Rainfall erosivity in south-central Nigeria. *Soil Technol.* 7 (4), 279–290.
- Salles, C., Poesen, J., Sempere-Torres, D., 2002. Kinetic energy of rain and its functional relationship with intensity. *J. Hydrol.* 257 (1), 256–270.
- Segura, C., Sun, G., McNulty, S., Zhang, Y., 2014. Potential impacts of climate change on soil erosion vulnerability across the conterminous United States. *J. Soil Water Conserv.* 69 (2), 171–181.
- Serdeczny, O., et al., 2017. Climate change impacts in Sub-Saharan Africa: from physical changes to their social repercussions. *Reg. Environ. Chang.* 17 (6), 1585–1600.
- Smithen, A., Schulze, R., 1982. The spatial distribution in southern Africa of rainfall erosivity for use in the Universal Soil Loss Equation. *Water SA* 8 (2), 74–78.
- Sylla, M.B., Nikiema, P.M., Gibba, P., Kebe, I., Klutse, N.A.B., 2016. Climate Change Over West Africa: Recent Trends and Future Projections, Adaptation to Climate Change and Variability in Rural West Africa. Springer, pp. 25–40.
- Taylor, K.E., Stouffer, R.J., Meehl, G.A., 2012. An overview of CMIP5 and the experiment design. *Bull. Am. Meteorol. Soc.* 93 (4), 485–498.
- Ufoegbune, G., et al., 2011. Rainfall erosivity pattern of Ogun river basin area (Nigeria) using modified Fournier index. *Eur. Water* 35, 23–29.
- Vrieling, A., Hoedjes, J.C., van der Velde, M., 2014. Towards large-scale monitoring of soil erosion in Africa: accounting for the dynamics of rainfall erosivity. *Glob. Planet. Chang.* 115, 33–43.
- Wischmeier, W.H., Smith, D.D., 1978. Predicting Rainfall Erosion Losses - A Guide to Conservation Planning. Predicting Rainfall Erosion Losses - A Guide to Conservation Planning.
- Wischmeier, W., 1968. Erosion Rates and Contributing Factors in Semi-arid Regions. International Seminar on Water and Soil Utilisation. South Dakota, Brookings.
- Yan, D., Werners, S.E., Ludwig, F., Huang, H.Q., 2015. Hydrological response to climate change: the Pearl River, China under different RCP scenarios. *J. Hydrol. Reg. Stud.* 4, 228–245.
- Yang, D., Kanae, S., Oki, T., Koike, T., Musiak, K., 2003. Global potential soil erosion with reference to land use and climate changes. *Hydrol. Process.* 17 (14), 2913–2928.
- Zhou, P., Luukkanen, O., Tokola, T., Nieminen, J., 2008. Effect of vegetation cover on soil erosion in a mountainous watershed. *Catena* 75 (3), 319–325.